Supporting Information

# Combustion activation induced solid-state synthesis for N, B co-doped carbon/zinc borate anode with a boosting of sodium storage performance

*Hao Zhang, Dingyue Zhang, Mingyi Guo, Zheng Huang, Xu Wang, Caiqin Gao, Fan Gao, Mauricio Terrones, and Yanqing Wang**

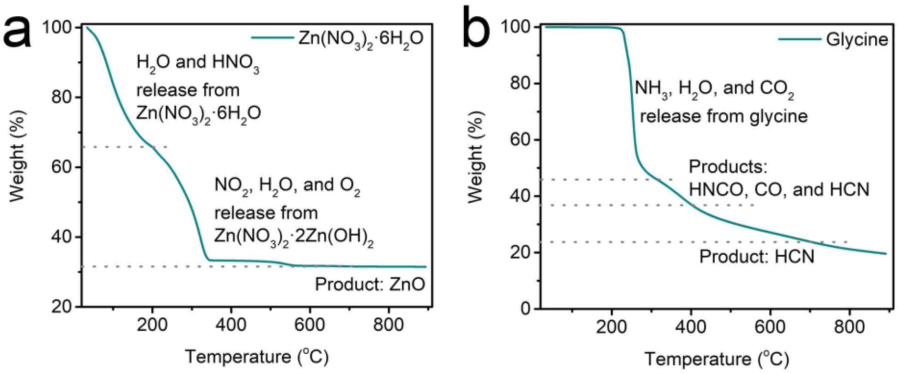


**Figure S1.** TG curves of a) $Zn(NO_3)_2{\cdot}6H_2O$ and b) glycine.

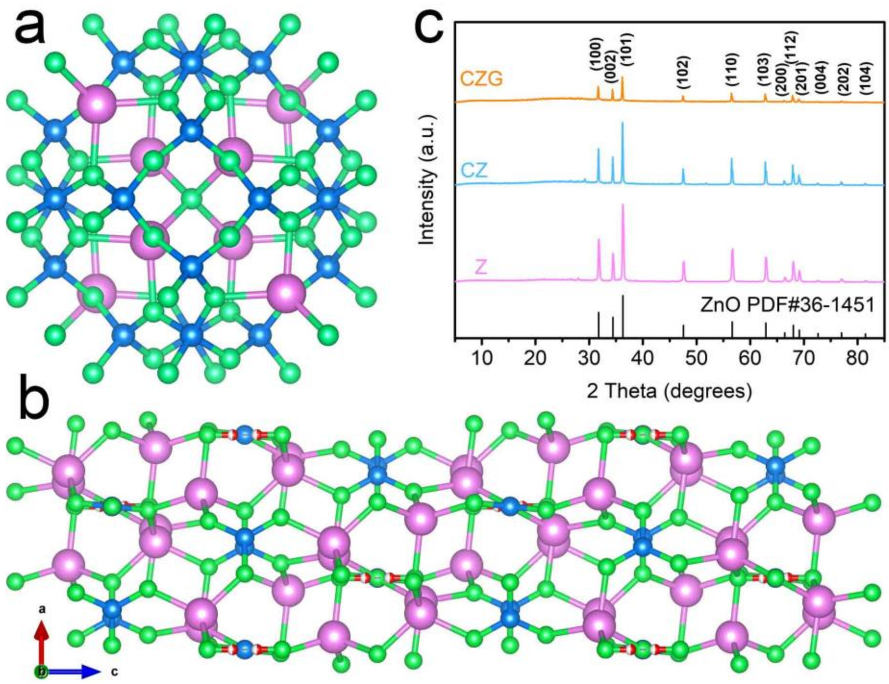


**Figure S2.** Crystal structure of a) $Zn_4O(BO_2)_6$ and b) $Zn_6O(OH)(BO_3)_3$ viewed along b-axis. c) XRD patterns of Z, CZ, and CZG.

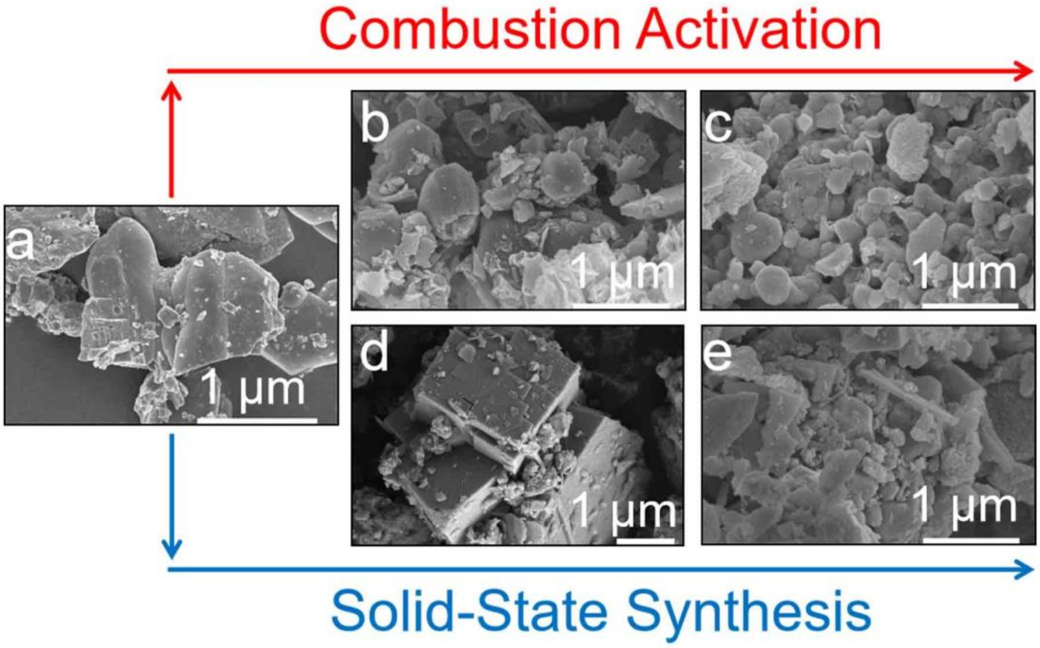


**Figure S3.** SEM images of a) Z, b) CZ, c) CZG, d) BZ, and e) CBZ.

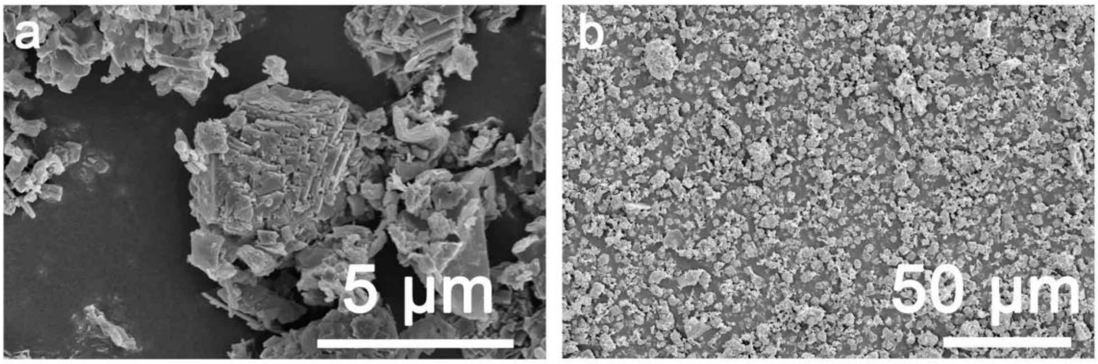


**Figure S4.** Lower magnification SEM images of CBZG.

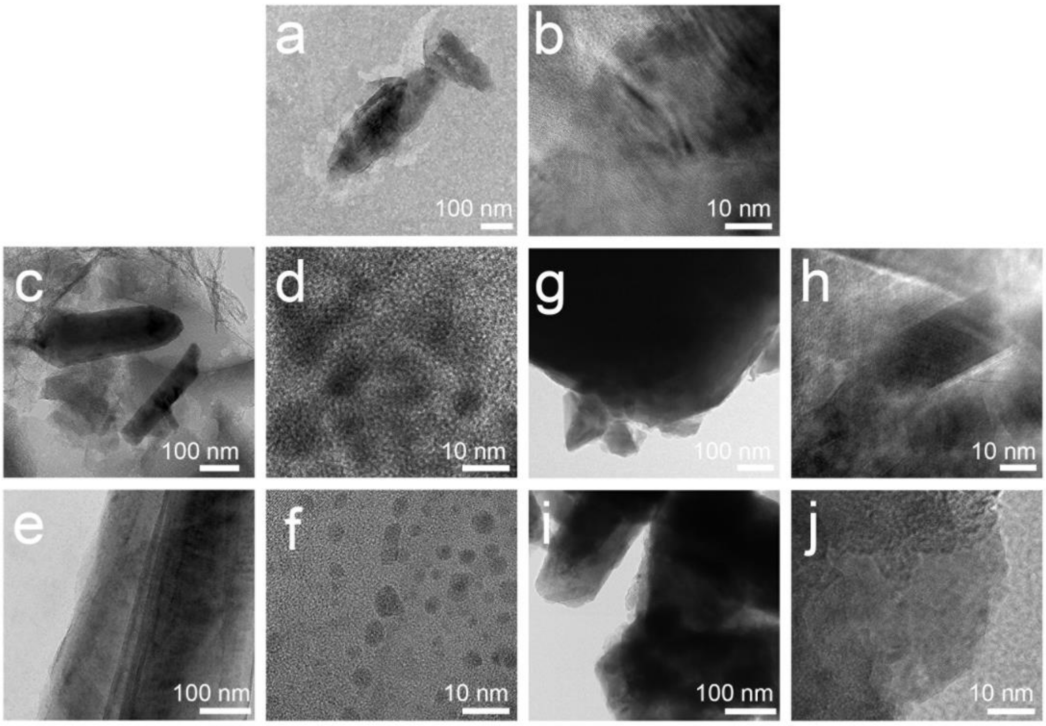


**Figure S5.** TEM and high-resolution TEM images of a, b) Z, c, d) CZ, e, f) CZG, g, h) BZ, and i, j) CBZ.

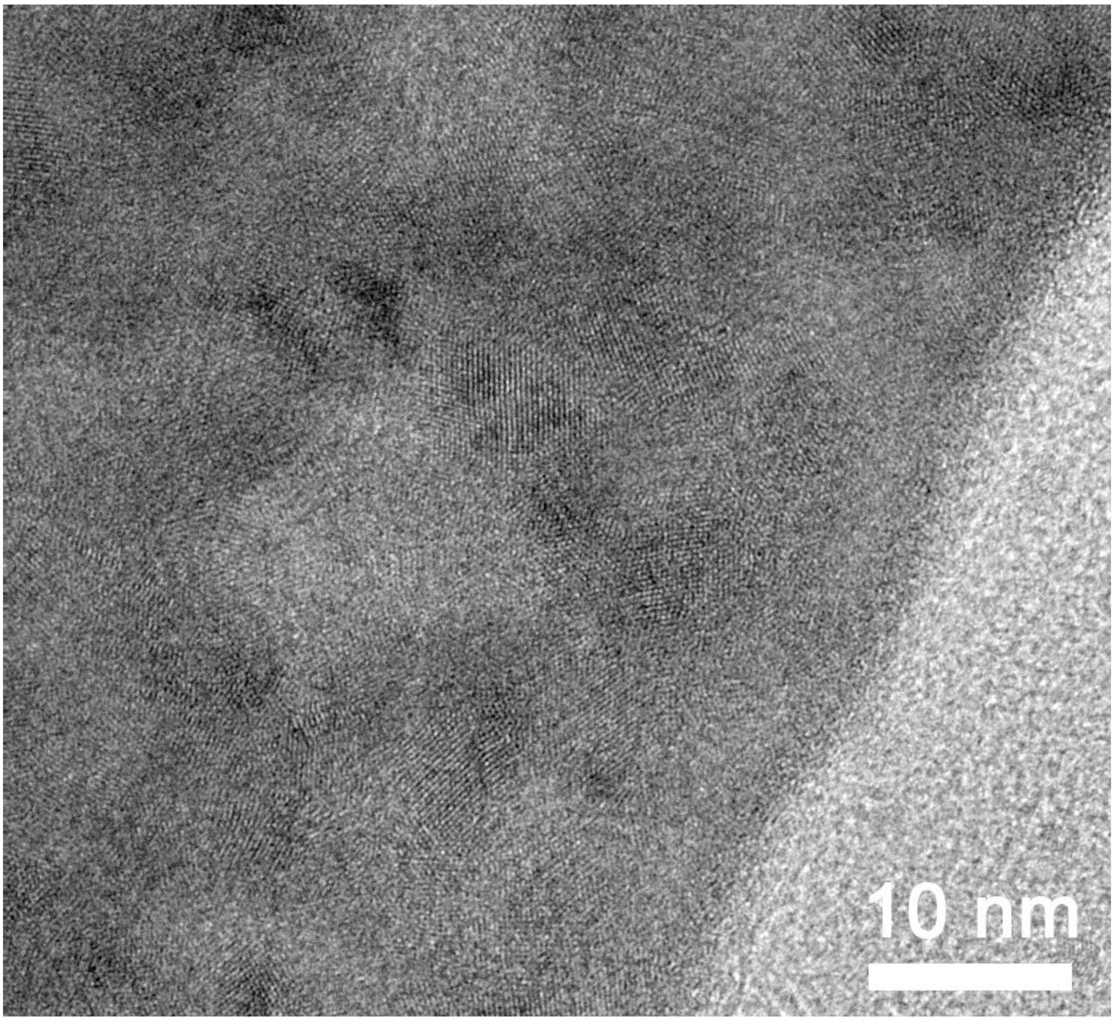


**Figure S6.** High-resolution TEM image of CBZG.

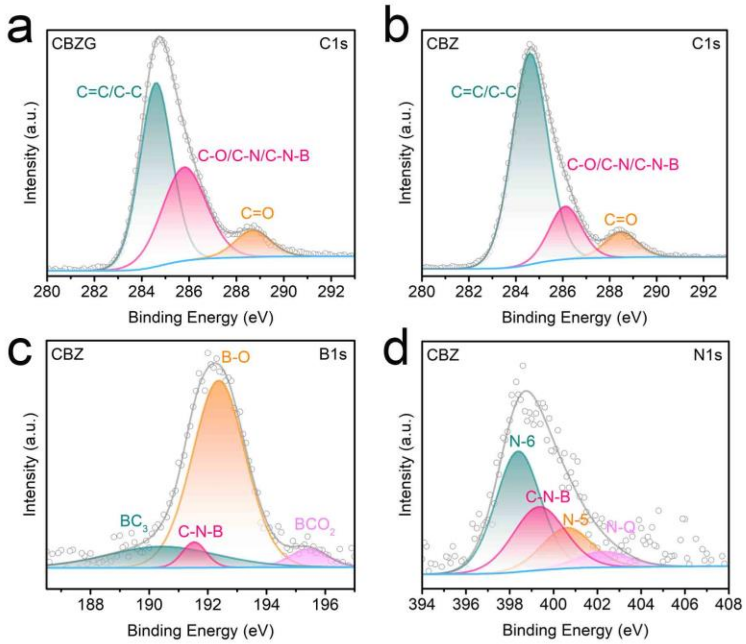


**Figure S7.** High-resolution C 1s XPS spectra of a) CBZG and b) CBZ. c, d) High-resolution B 1s and N 1s XPS spectra of CBZ.

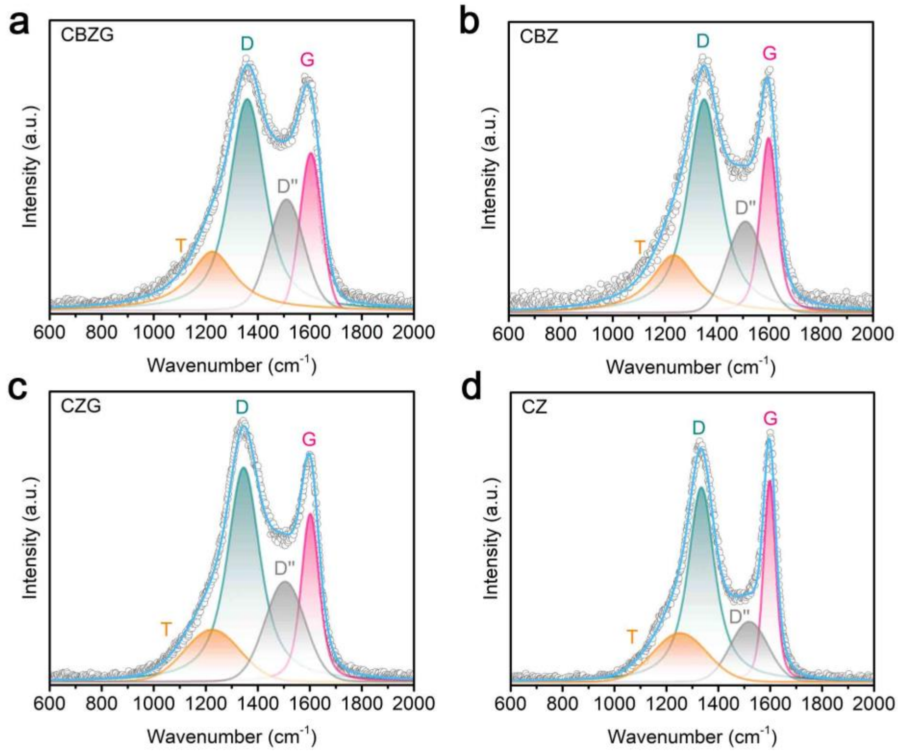


**Figure S8.** Fitted Raman spectra of a) CBZG, b) CBZ, c) CZG, d) CZ.

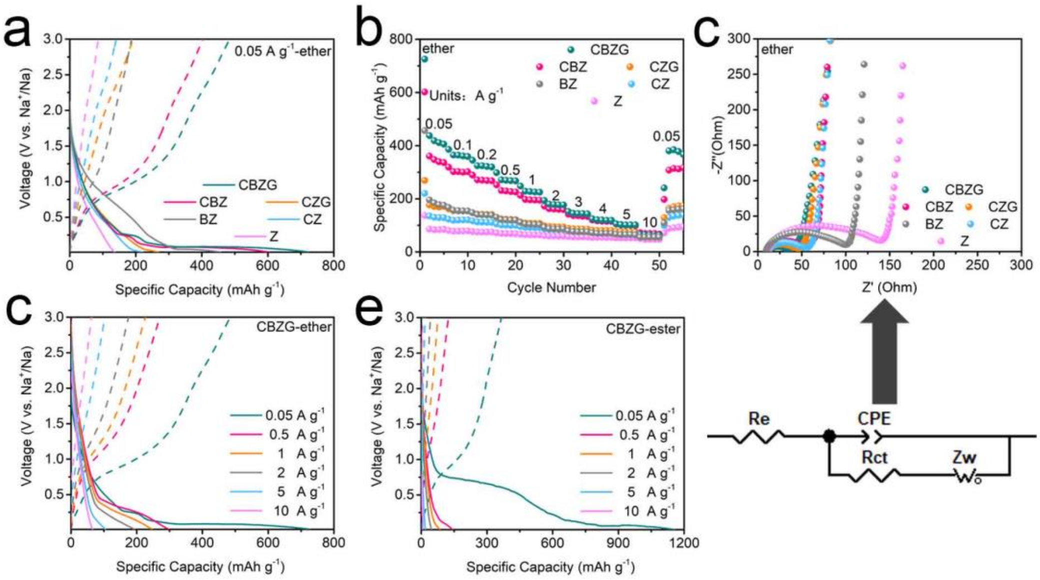


**Figure S9.** $Na^+$ storage performance of the obtained materials as the half-cell anode in ether- or ester-based electrolyte. a) Discharge/charge profiles at 0.05 A $g^{-1}$. b) Rate capability. c) Nyquist plots and equivalent circuit. d, e) Discharge/charge profiles at different current densities of CBZG.

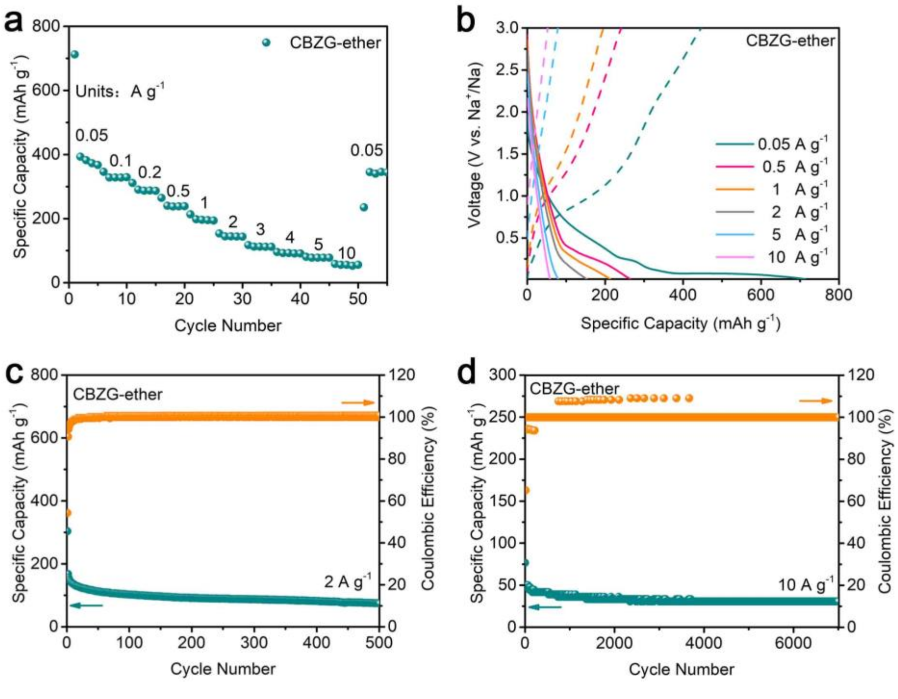


**Figure S10.** $Na^+$ storage performance of CBZG as the half-cell anode with a higher mass loading of ~2.0 mg $cm^{-2}$ in ether-based electrolyte. a) Rate capability. b) Discharge/charge profiles at different current densities. Cycling performance at c) 2 A $g^{-1}$ and d) 10 A $g^{-1}$.

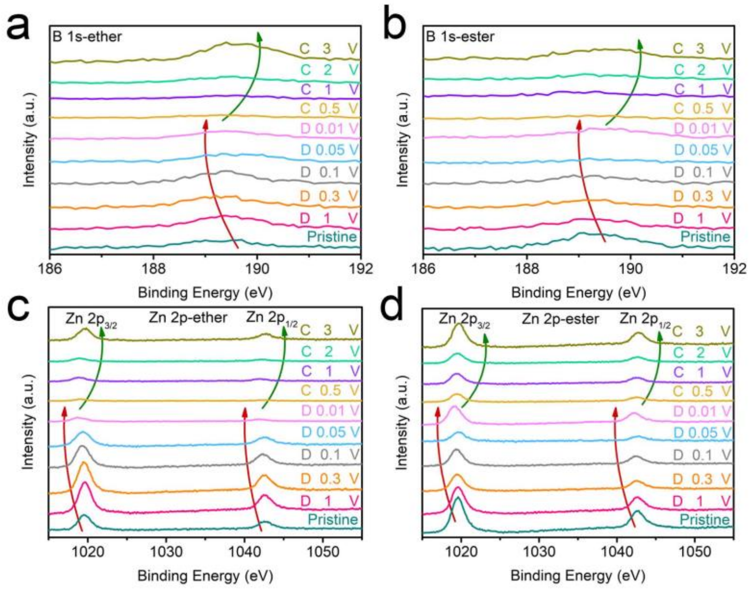


**Figure S11.** $Na^+$ storage process analysis of CBZG as the half-cell anode in ether- or ester-based electrolyte. Ex situ high-resolution XPS analysis at various stages for a, b) B 1s and c, d) Zn 2p.

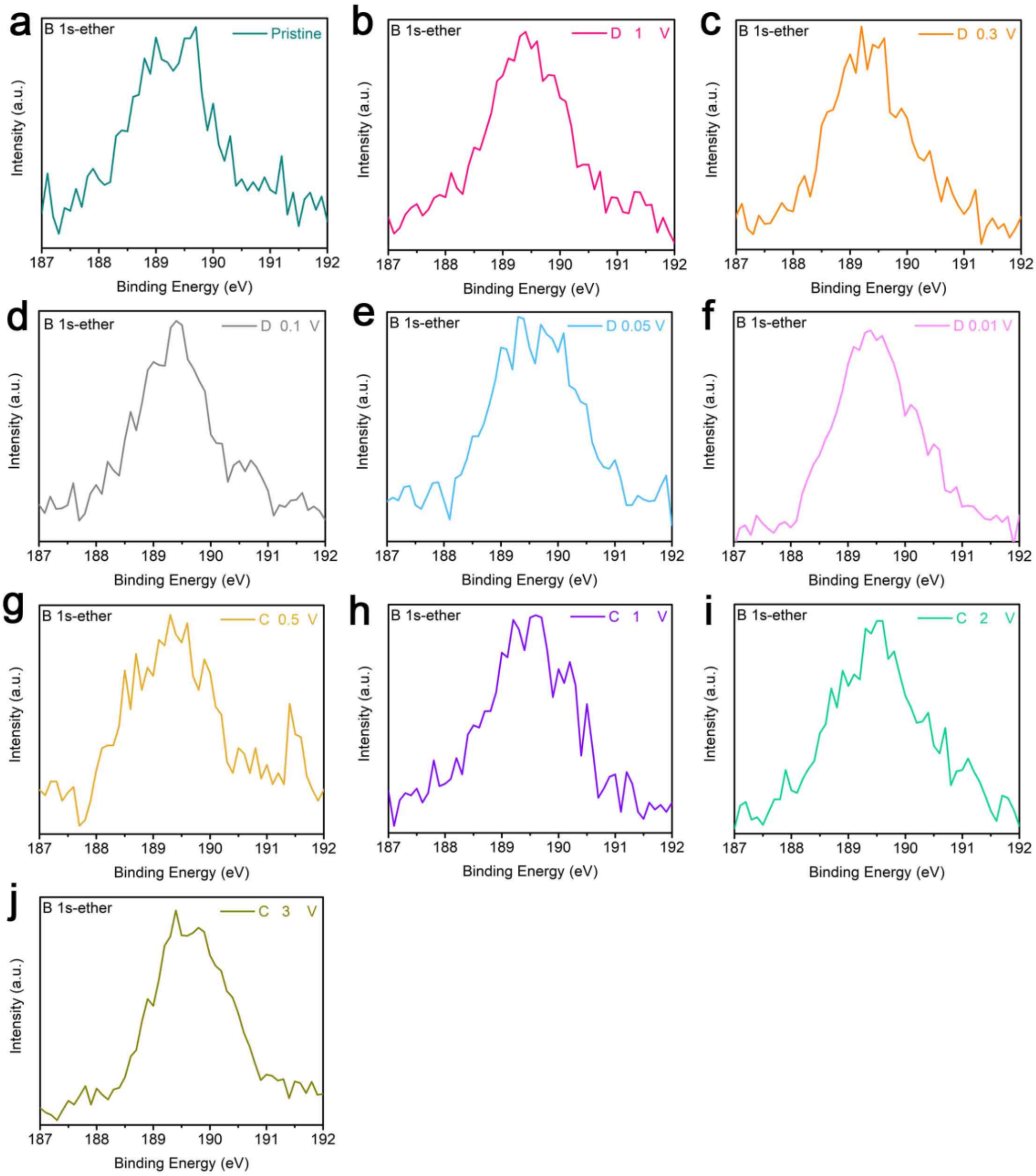


**Figure S12.** Ex situ high-resolution XPS analysis at various stages for B 1s in ether-based electrolyte.

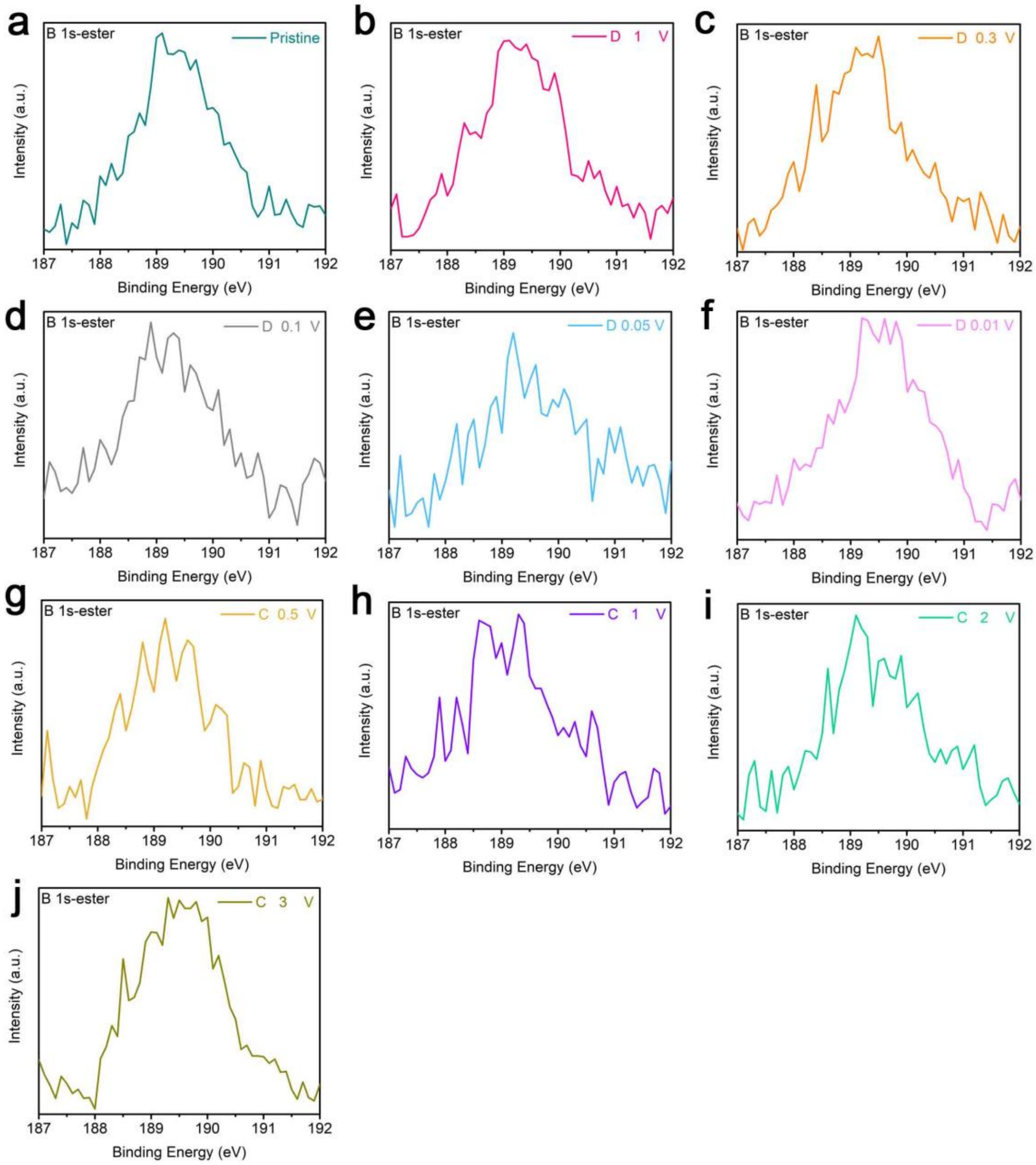


**Figure S13.** Ex situ high-resolution XPS analysis at various stages for B 1s in ester-based electrolyte.

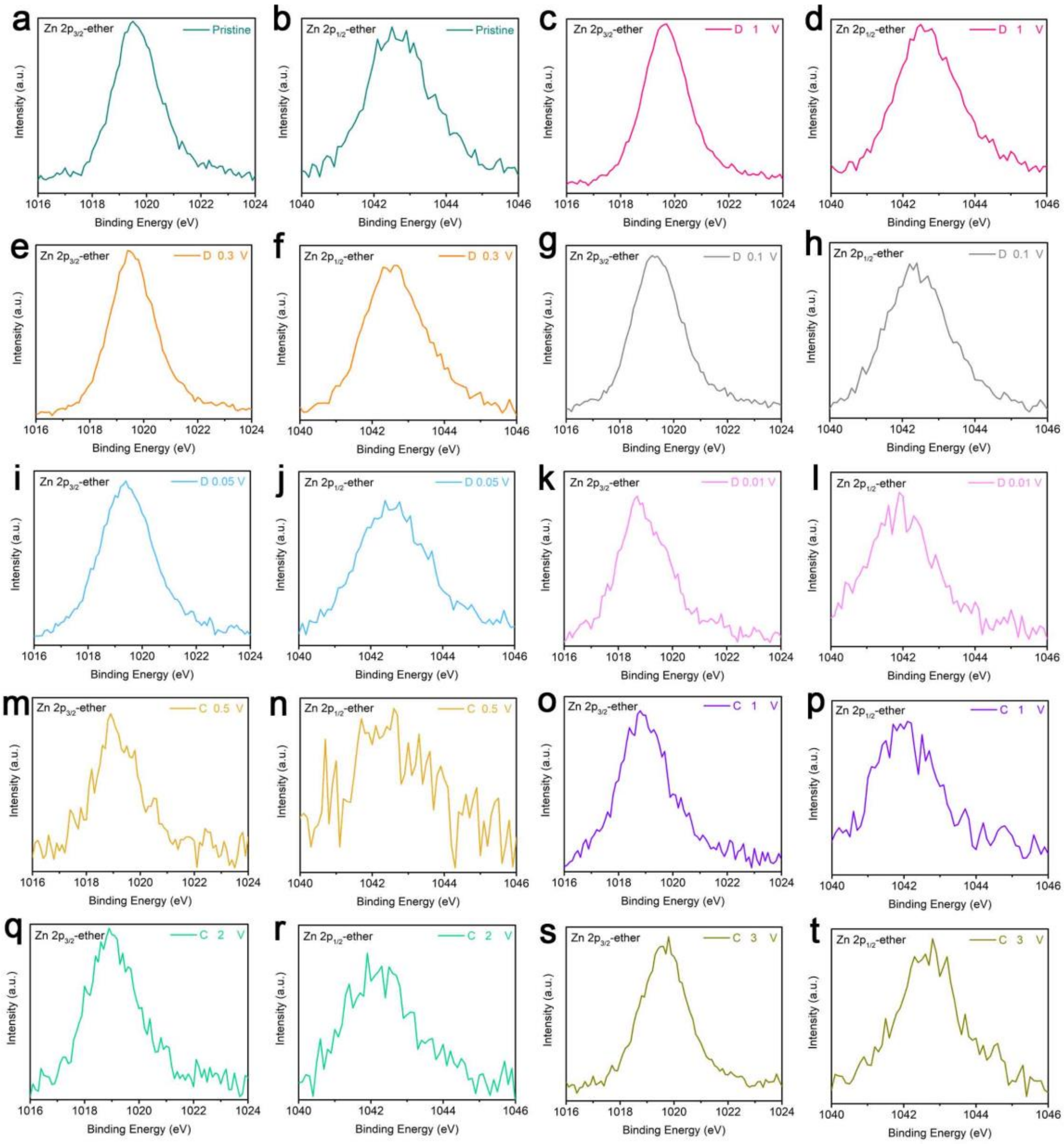


**Figure S14.** Ex situ high-resolution XPS analysis at various stages for Zn 2p in ether-based electrolyte.

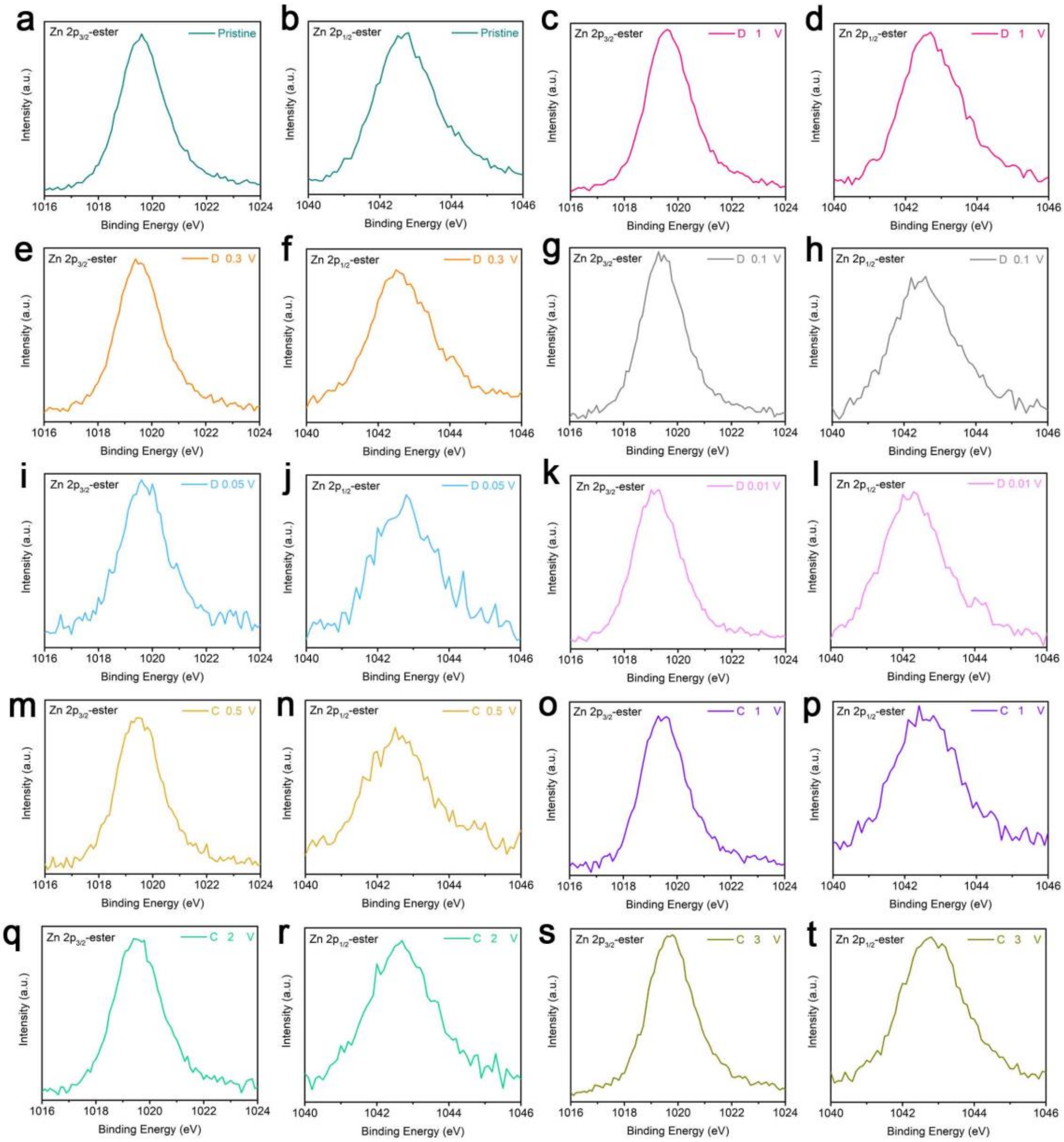


**Figure S15.** Ex situ high-resolution XPS analysis at various stages for Zn 2p in ester-based electrolyte.

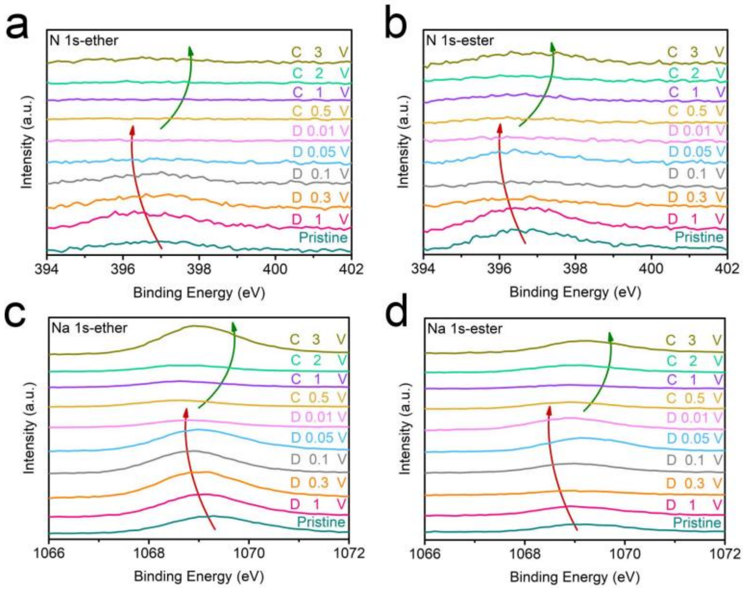


**Figure S16.** $Na^+$ storage process analysis of CBZG as the half-cell anode in ether- or ester-based electrolyte. Ex situ high-resolution XPS analysis at various stages for a, b) N 1s and c, d) Na 1s.

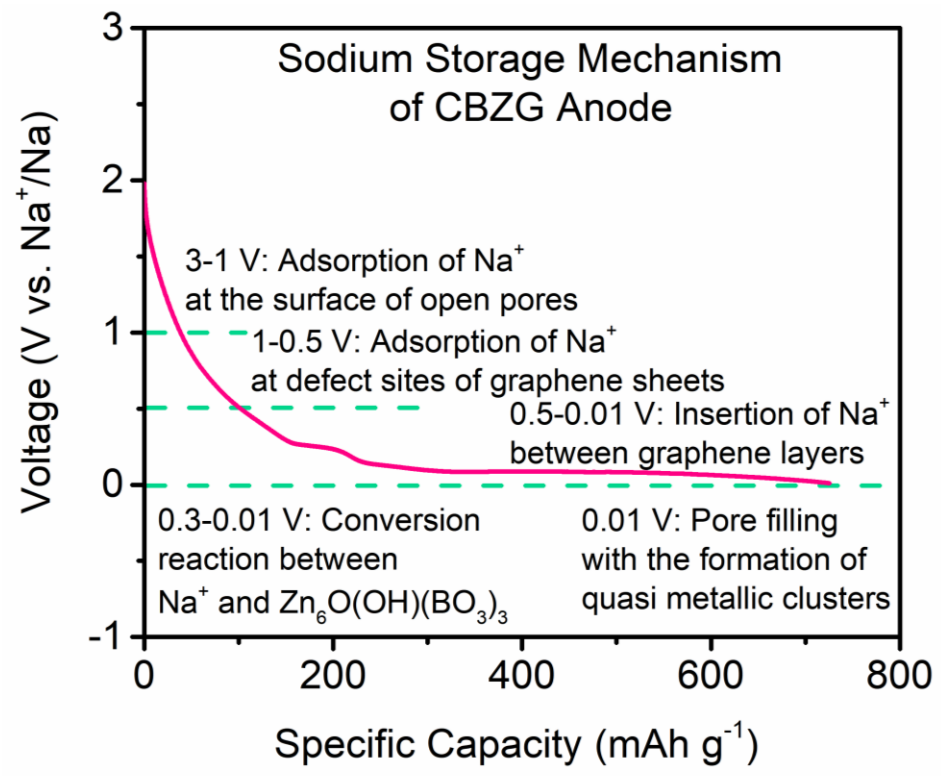


**Figure S17.** The sodium storage mechanism of CBZG anode.

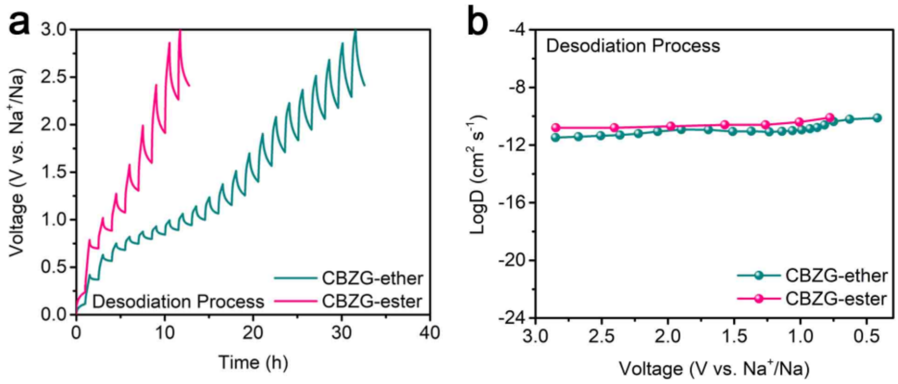


**Figure S18.** a) GITT potential profiles with a pulse current of 0.05 A $g^{-1}$ for 0.5 h, followed by a 1.0 h relaxation process. b) $Na^+$ diffusion coefficients calculated from the GITT potential profiles for the charge process.

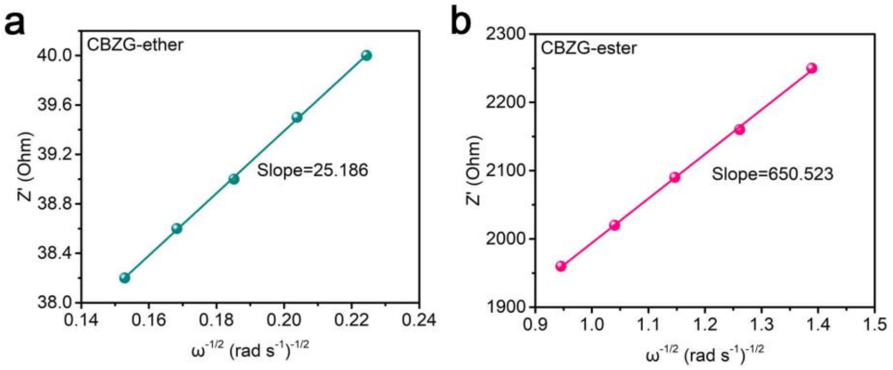


**Figure S19.** $\sigma$ values (slope of the plot of Z' versus $\omega^{-1/2}$) of CBZG anode in a) ether-based electrolyte and b) ester-based electrolyte.

The diffusion coefficients of $Na^+$ ions were calculated from Electrochemical impedance spectra (EIS) according to the following equation [1]:

$$D_{Na^+} = \frac{R^2T^2}{2A^2n^4F^4C^2\sigma^2}$$

Where $R$ is the gas constant, $T$ is the Kelvin temperature, $A$ is the electrode area, $n$ is the number of electrons per molecule during the redox reaction, $F$ is the Faraday constant, and $C$ is the molar concentration of sodium ions. $\sigma$ is the Warburg coefficient, which can be obtained from the slope of the plot of Z' versus $\omega^{-1/2}$ in **Figure S19**.

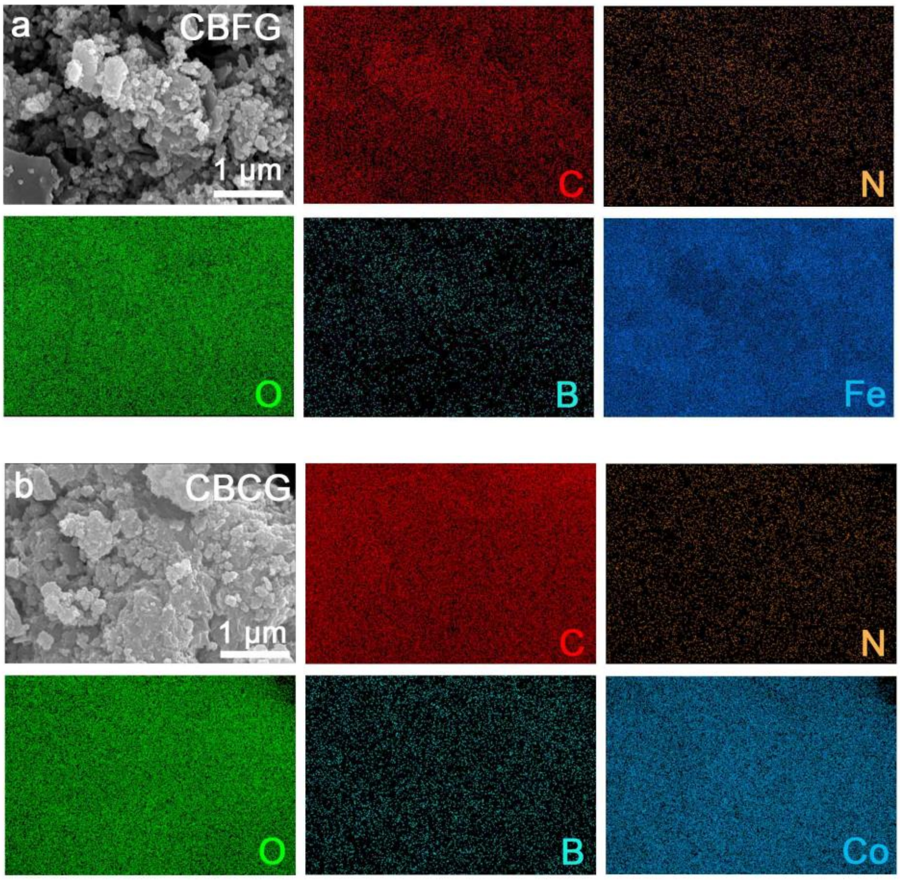


**Figure S20.** Element mapping images of a) CBFG and b) CBCG.

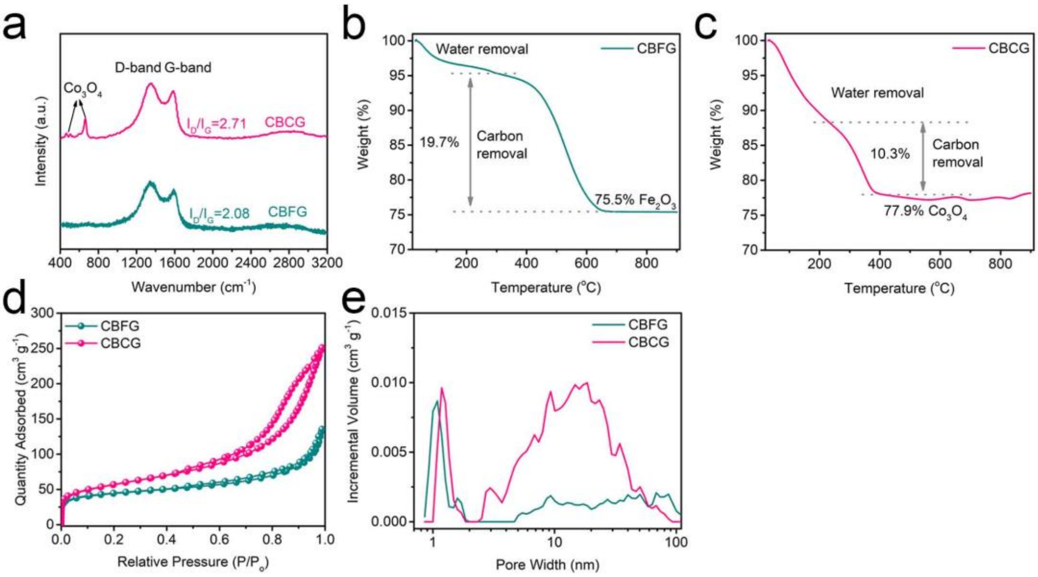


**Figure S21.** Structure characterizations of CBFG and CBCG. a) Raman spectra. TG curves of b) CBFG and c) CBCG. d) $N_2$ adsorption-desorption isotherms. e) Pore size distribution curves.

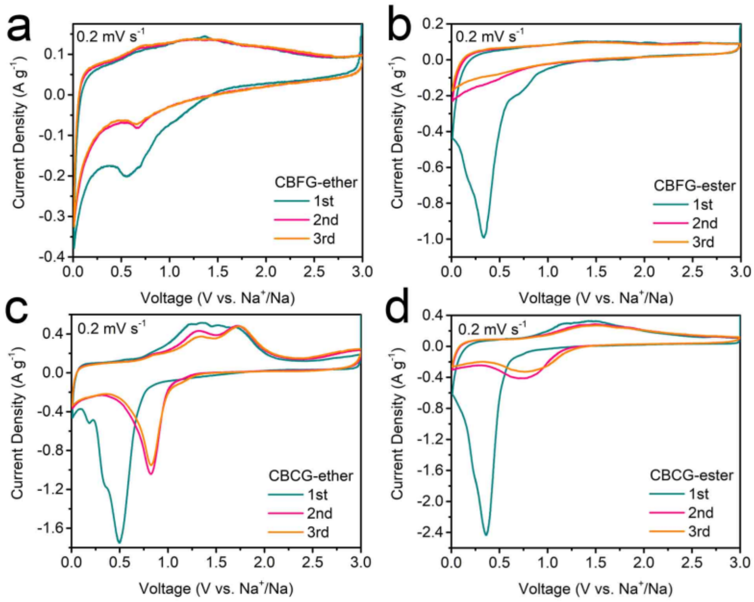


**Figure S22.** CV curves at 0.2 mV $s^{-1}$ of CBFG and CBCG as the half-cell anode in ether- or ester-based electrolyte.

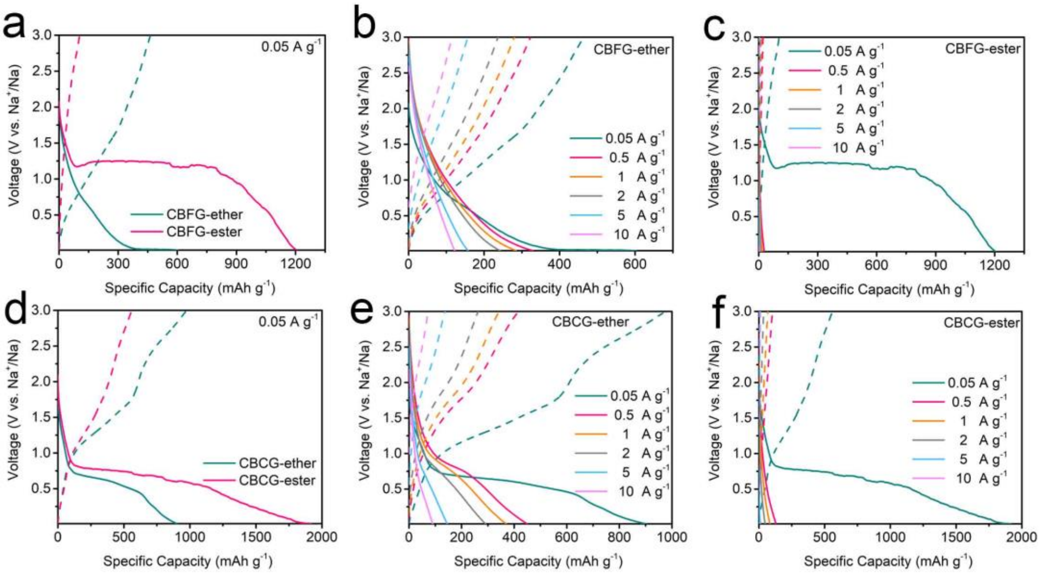


**Figure S23.** Discharge/charge profiles at different current densities of CBFG and CBCG as the half-cell anode in ether- or ester-based electrolyte.

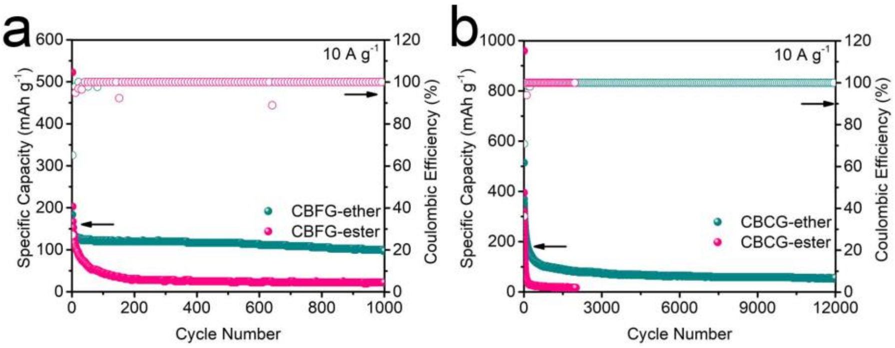


**Figure S24.** Cycling performance at 10 A $g^{-1}$ of CBFG and CBCG as the half-cell anode in ether- or ester-based electrolyte.

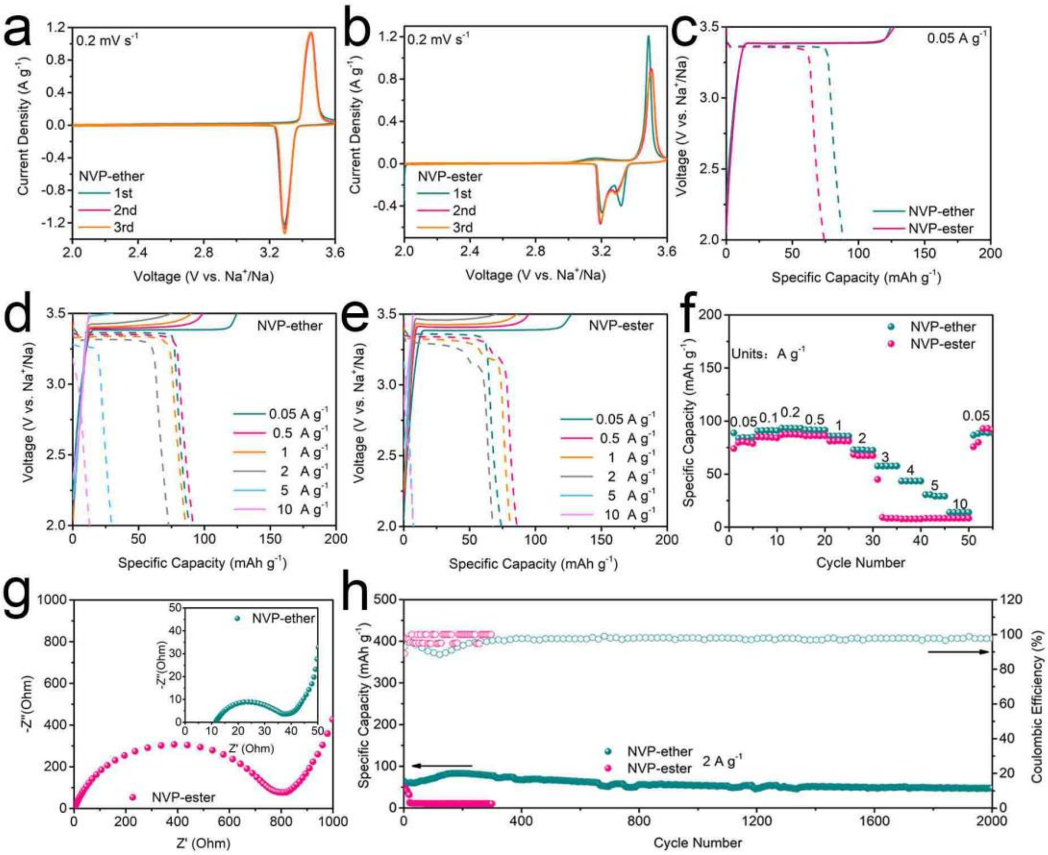


**Figure S25.** $Na^+$ storage performance of $Na_3V_2(PO_4)_3$ as the half-cell cathode in ether- or ester-based electrolyte. a, b) CV curves at 0.2 mV $s^{-1}$. c-e) Charge/discharge profiles at different current densities. f) Rate capability. g) Nyquist plots. h) Cycling performance at 2 A $g^{-1}$.

The sodium storage performance of commercial $Na_3V_2(PO_4)_3$ (NVP) cathode was also studied in ether- or ester-based electrolyte at 2-3.5/3.6 V. Ether-based electrolyte has higher ICE than ester-based electrolyte, confirmed by CV curves and the initial galvanostatic charge-discharge profiles at 0.05 A $g^{-1}$. In ether-based electrolyte, NVP cathode has rate capability of 88.8, 90.7, 93.3, 91.6, 85.9, 72.9, 57.5, 43.4, 30.6, 13.9, and 86.6 mAh $g^{-1}$ at 0.05, 0.1, 0.2, 0.5, 1, 2, 3, 4, 5, 10, and 0.05 A $g^{-1}$; in ester-based electrolyte, NVP cathode has rate capability of 74.0, 85.0, 87.1, 86.0, 81.1, 68.3, 9.2, 7.8, 8.3, 8.3, and 75.8 mAh $g^{-1}$ at the same current densities. NVP cathode has much lower $R_{ct}$ (23.7 Ω) in ether-based electrolyte than that in ester-based electrolyte (734.4 Ω). Due to the intercalation property of NVP cathode, $Na^+$ need to de-solvate first, and then intercalate into NVP cathode——the rate kinetics heavily hinge on the de-solvation rate.[2] Ether-based electrolyte shows a higher rate capability and lower $R_{ct}$ than ester-based electrolyte, which also manifests the faster de-solvation in ether-based electrolyte. NVP cathode in ether-based electrolyte possess a superior cycling performance after 2 000 cycles at 2 A $g^{-1}$ (84.7 % capacity retention), while in ester-based electrolyte has an inferior cycling performance below 300 cycles at 2 A $g^{-1}$ (capacity close to zero). Through the above electrochemical analyses of NVP cathode, we have proved the advantages of ether-based electrolyte in sodium storage performance, which is coherent with the analysis results of anodes.

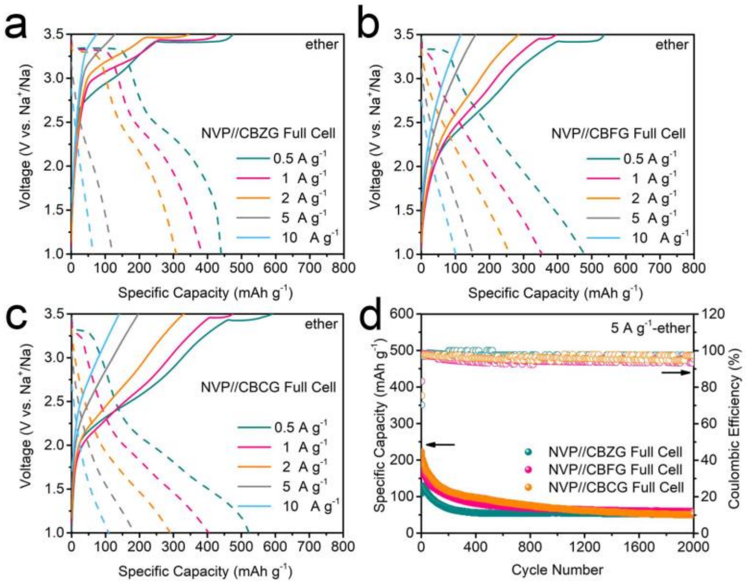


**Figure S26.** Charge/discharge profiles at different current densities of a) NVP//CBZG, b) NVP//CBFG, and c) NVP//CBCG sodium-ion full-cells in ether-based electrolyte. d) Cycling performance of sodium-ion full-cells at 5 A $g^{-1}$ in ether-based electrolyte.


**Figure S27.** a-c) Photos show that full-cells can light up LED bulbs.

**Table S1.** The contents of C, N, O, B, Zn, Fe and Co in obtained various materials.

| Samples | XPS composition (at%) | | | | | | |
|---|---|---|---|---|---|---|---|
| | C | N | O | B | Zn | Fe | Co |
| CBZG | 64.00 | 5.01 | 20.59 | 6.31 | 4.09 | - | - |
| CBZ | 61.37 | 1.87 | 24.93 | 6.07 | 5.76 | - | - |
| BZ | - | - | 44.00 | 18.22 | 13.31 | - | - |
| CZG | 77.77 | 2.33 | 16.54 | - | 3.36 | - | - |
| CZ | 79.29 | - | 17.06 | - | 3.65 | - | - |
| CBFG | 62.99 | 2.84 | 23.77 | 1.69 | - | 8.70 | - |
| CBCG | 52.17 | 0.47 | 33.64 | 4.88 | - | - | 8.85 |

**Table S2.** The fitting results of high-resolution XPS B 1s and N 1s for CBZG and CBZ.

| Samples | B 1s (%) | | | | N 1s (%) | | | |
|---|---|---|---|---|---|---|---|---|
| | $BC_3$ | C-N-B | B-O | $BCO_2$ | N-6 | C-N-B | N-5 | N-Q |
| CBZG | 13.50 | 16.40 | 68.83 | 1.27 | 27.13 | 33.15 | 24.64 | 15.08 |
| CBZ | 17.25 | 4.56 | 73.08 | 5.11 | 46.77 | 28.59 | 17.49 | 7.15 |

**Table S3.** The specific surface area and pore volume of the obtained various materials.

| Samples | $S_{BET}$ ($m^2$ $g^{-1}$) | $V_t$ ($cm^3$ $g^{-1}$) |
|---|---|---|
| CBZG | 79 | 0.047 |
| CBZ | 36 | 0.028 |
| BZ | 0.4 | 0.002 |
| CZG | 238 | 0.116 |
| CZ | 70 | 0.055 |
| Z | 4 | 0.006 |
| CBFG | 159 | 0.151 |
| CBCG | 202 | 0.325 |

**Table S4.** $R_e$ value and the $R_{ct}$ value obtained from the equivalent circuit diagrams for various electrodes.

| Electrolytes | Samples | $R_e$ (Ω) | $R_{ct}$ (Ω) |
|---|---|---|---|
| Ether | CBZG | 11.4 | 21.9 |
| | CBZ | 10.7 | 39.3 |
| | BZ | 8.9 | 80.5 |
| | CZG | 11.1 | 31.3 |
| | CZ | 11.0 | 39.8 |
| | Z | 10.3 | 113.3 |
| | CBFG | 11.1 | 20.0 |
| | CBCG | 11.0 | 12.1 |
| | NVP//CBZG | 12.2 | 24.2 |
| | NVP//CBFG | 9.9 | 33.8 |
| | NVP//CBCG | 9.9 | 26.0 |
| Ester | CBZG | 4.5 | 1123.0 |
| | CBFG | 5.0 | 1636.0 |
| | CBCG | 4.3 | 2084.0 |

**Table S5.** The rate capability of CBFG and CBCG in ether- and ester-based electrolytes.

| Samples | Capacity (mAh $g^{-1}$) | | | | | | | | | |
|---|---|---|---|---|---|---|---|---|---|---|
| | 0.05 A $g^{-1}$ | 0.1 A $g^{-1}$ | 0.2 A $g^{-1}$ | 0.5 A $g^{-1}$ | 1 A $g^{-1}$ | 2 A $g^{-1}$ | 3 A $g^{-1}$ | 4 A $g^{-1}$ | 5 A $g^{-1}$ | 10 A $g^{-1}$ |
| CBFG-ether | 460.5 | 415.2 | 377.9 | 329.9 | 285.1 | 243.0 | 205.1 | 177.9 | 158.4 | 122.3 |
| CBCG-ether | 690.6 | 589.7 | 527.4 | 449.5 | 370.1 | 291.1 | 225.9 | 178.9 | 145.8 | 91.7 |
| CBFG-ester | 193.4 | 81.6 | 52.1 | 28.2 | 17.8 | 9.5 | 5.8 | 4.4 | 4.2 | 4.2 |
| CBCG-ester | 690.6 | 364.6 | 205.1 | 130.2 | 83.9 | 47.3 | 27.5 | 17.8 | 12.5 | 5.6 |

**Table S6.** The capacity of $C/Fe_2O_3$ and $C/Co/Co_3O_4$ electrodes in comparison with previous iron oxide or cobalt oxide based works.

| Sample | Capacity |
|---|---|
| **$C/Fe_2O_3$ (This work)** | 460.5 mAh $g^{-1}$ at 0.05 A $g^{-1}$<br>158.4 mAh $g^{-1}$ at 5 A $g^{-1}$ |
| $GFe_2O_3$-5[3] | 445 mAh $g^{-1}$ at 0.5 A $g^{-1}$<br>129 mAh $g^{-1}$ at 5 A $g^{-1}$ |
| $Fe_2O_3$:Ge NFs[4] | 320 mAh $g^{-1}$ at 0.05 A $g^{-1}$<br>140 mAh $g^{-1}$ at 2 A $g^{-1}$ |
| α- $Fe_2O_3$:Mn@rGO[5] | 56 mAh $g^{-1}$ at 1 A $g^{-1}$ |
| $4Fe_3O_4$-CNFs[6] | 431.1 mAh $g^{-1}$ at 0.1 A $g^{-1}$ |

**Table S7.** The rate capability of NVP//CBZG, NVP//CBFG, and NVP//CBCG full-cells in ether-based

| | |
|---|---|
| α-$Fe_2O_3$/γ-$Fe_2O_3$/Fe/C[7] | 301 mAh $g^{-1}$ at 0.1 A $g^{-1}$ |
| $Fe_2O_3$@C[8] | 434.4 mAh $g^{-1}$ at 0.2 A $g^{-1}$ |
| Ag@$Fe_3O_4$[9] | 278 mAh $g^{-1}$ at 0.2 C |
| $Fe_2O_3$-AHP[10] | 354.3 mAh $g^{-1}$ at 0.1 A $g^{-1}$ |
| $Fe_3O_4$@C/rGO[11] | 366 mAh $g^{-1}$ at 0.1 A $g^{-1}$<br>125 mAh $g^{-1}$ at 5 A $g^{-1}$ |
| $Fe_2O_3$/NGC[12] | 404.6 mAh $g^{-1}$ at 0.25 A $g^{-1}$ |
| **C/Co/$Co_3O_4$ (This work)** | 690.6 mAh $g^{-1}$ at 0.05 A $g^{-1}$<br>291.1 mAh $g^{-1}$ at 2 A $g^{-1}$ |
| $Co_3O_4$/N-CNS[13] | 533 mAh $g^{-1}$ at 0.05 A $g^{-1}$<br>191 mAh $g^{-1}$ at 1 A $g^{-1}$ |
| 3D-CoO-NrGO[14] | 445 mAh $g^{-1}$ at 0.025 A $g^{-1}$<br>135 mAh $g^{-1}$ at 5 A $g^{-1}$ |
| Cu-$Co_3O_4$@Void@NC[15] | 501 mAh $g^{-1}$ at 0.2 A $g^{-1}$<br>301 mAh $g^{-1}$ at 2 A $g^{-1}$ |
| $Co_3O_4$@N-CNFs[16] | 520 mAh $g^{-1}$ at 0.1 A $g^{-1}$<br>205 mAh $g^{-1}$ at 3.2 A $g^{-1}$ |
| $ZnCo_2O_4$/RGO[17] | 447.53 mAh $g^{-1}$ at 0.1 A $g^{-1}$<br>214.73 mAh $g^{-1}$ at 1.6 A $g^{-1}$ |
| $NiCo_2O_4$/CTBs[18] | 473 mAh $g^{-1}$ at 0.1 A $g^{-1}$<br>236 mAh $g^{-1}$ at 5 A $g^{-1}$ |
| $Zn_xCo_{3-x}O_4$[19] | 345 mAh $g^{-1}$ at 0.2 A $g^{-1}$<br>142 mAh $g^{-1}$ at 2 A $g^{-1}$ |
| $CoMoO_4$[20] | 231.3 mAh $g^{-1}$ at 0.2 A $g^{-1}$<br>131.6 mAh $g^{-1}$ at 2 A $g^{-1}$ |

| | |
|---|---|
| $Fe_{0.8}CoMnO_4$[21] | 396 mAh $g^{-1}$ at 0.2 A $g^{-1}$<br>234 mAh $g^{-1}$ at 2 A $g^{-1}$ |
| $Co_3O_4/ZnO$[22] | 242 mAh $g^{-1}$ at 2 A $g^{-1}$ |

electrolytes.

| Samples | Capacity (mAh $g^{-1}$) | | | | | | |
|---|---|---|---|---|---|---|---|
| | 0.5 A $g^{-1}$ | 1 A $g^{-1}$ | 2 A $g^{-1}$ | 3 A $g^{-1}$ | 4 A $g^{-1}$ | 5 A $g^{-1}$ | 10 A $g^{-1}$ |
| NVP//CBZG | 440.1 | 385.2 | 309.1 | 231.8 | 142.3 | 122.3 | 66.7 |
| NVP//CBFG | 478.7 | 354.3 | 260.6 | 211.0 | 176.7 | 152.8 | 102.8 |
| NVP//CBCG | 522.5 | 403.9 | 291.4 | 245.2 | 211.3 | 184.8 | 111.2 |

**References**

[1] S. Huang, D. Yang, X. Qiu, W. Zhang, Y. Qin, C. Wang, C. Yi, Adv. Funct. Mater. 2022, *32*, 2203279.

[2] X. Yi, X. Li, J. Zhong, S. Wang, Z. Wang, H. Guo, J. Wang, G. Yan, *Adv. Funct. Mater.* **2022**, *32*, 2209523.

[3] Y. Zhang, Q. Wang, K. Zhu, K. Ye, G. Wang, D. Cao, J. Yan, *Chem. Eng. J.* **2022**, *428*, 131204.

[4] B. Petrovičovà, C. Ferrara, G. Brugnetti, C. Ritter, M. Fracchia, P. Ghigna, S. Pollastri, C. Triolo, L. Spadaro, R. Ruffo, S. Santangelo, *Appl. Sci.* **2021**, *11*, 1483.

[5] V. Modafferi, C. Triolo, M. Fiore, A. Palella, L. Spadaro, N. Pianta, R. Ruffo, S. Patane, S. Santangelo, M. G. Musolino, *Nanomaterials (Basel)* **2020**, *10*, 1588.

[6] Y. Huang, J. Zhou, Y. Zhang, L. Yan, S. Bao, Y. Yin, J. Lu, *J. Alloys Compd.* **2022**, *918*, 165672.

[7] L. Yin, Y. Pan, M. Li, Y. Zhao, S. Luo, *Nanotechnology* **2020**, *31*, 155402.

[8] C. Li, H. Su, K. Zhang, Z. Liu, H. Wang, D. Li, *J. Alloys Compd.* **2021**, *858*, 157714.

[9] D. Liu, C. Wang, K.-J. Jeong, J. Lee, *J. Alloys Compd.* **2020**, *832*, 152824.

[10] T. Li, H. Li, A. Qin, D. Zhang, F. Xu, *J. Power Sources* **2021**, *489*, 229510.

[11] J.-L. Xu, X. Zhang, Y.-X. Miao, M.-X. Wen, W.-J. Yan, P. Lu, Z.-R. Wang, Q. Sun, *Appl. Surf. Sci.* **2021**, *546*, 149163.

[12] J. Song, A. Y. Maulana, H. Kim, B. Yun, H. Gim, Y. Jeong, N. An, C. M. Futalan, J. Kim, *J. Alloys Compd.* **2022**, *921*, 166082.

[13] R. Li, L. Qing, W. Zhao, Y. k. Wu, J. Chen, W. Su, *Ionics* **2022**, *28*, 2613.

[14] W. Feng, V. S. Avvaru, R. R. Maca, S. J. Hinder, M. C. Rodriguez, V. Etacheri, *ACS Appl. Mater. Interfaces* **2021**, *13*, 27999.

[15] H. Kong, Y. Wu, W. Hong, C. Yan, Y. Zhao, G. Chen, *Energy Storage Mater.* **2020**, *24*, 610.

[16] L. Li, Q. Wang, X. Zhang, L. Fang, X. Li, W. Zhang, *Appl. Surf. Sci.* **2020**, *508*, 145295.

[17] Z. Zhang, Y. Huang, X. Liu, X. Wang, P. Liu, *Electrochim. Acta* **2020**, *342*, 136104.

[18] J. Zhao, C. Zhou, Y. Li, K. Cheng, K. Zhu, K. Ye, J. Yan, D. Cao, Y. Xie, G. Wang, *Int. J. Energy Res.* **2020**, *44*, 3883.

[19] M. Wang, Y. Huang, Y. Zhu, N. Zhang, J. Zhang, X. Qin, H. Zhang, *Electrochim. Acta* **2020**, *335*, 135694.

[20] J. Singh, S. Lee, P. Yadav, S. Kim, J. Kim, A. K. Rai, *ACS Appl. Energy Mater.* **2021**, *5*, 126.

[21] L. Wu, J. O. Yang, S. Guo, L. Yao, H. Li, S. Zhang, H. Yue, K. Cai, C. Zhang, C. Yang, Y. Cao, *Adv. Funct. Mater.* **2020**, *30*, 2001718.

[22] G. Fang, J. Zhou, Y. Cai, S. Liu, X. Tan, A. Pan, S. Liang, *J. Mater. Chem. A* **2017**, *5*, 13983.